Longitudinal Developmental Trajectories of Functional Connectivity Reveal Regional Distribution of Distinct Age Effects in Infancy

Supplementary Material

Table of Contents

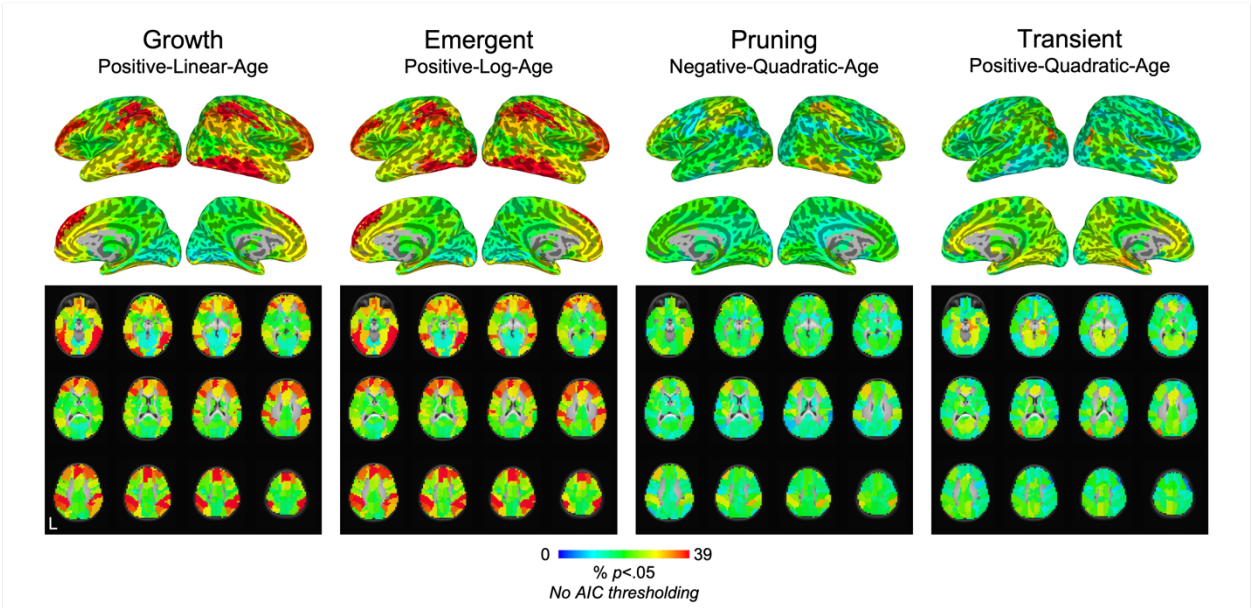

Figure S1. Heatmaps of age effects without AIC thresholding. Qualitatively, heatmaps show unique patterns of age effects on brain connectivity across the first two years of life corresponding to growth (positive-linear-age), emergent (positive-log-age), pruning (negative-quadratic-age), and transient (positive-quadratic-age) effects. There is significant overlap between the growth and emergent models in the absence of AIC thresholding. The color map and value of each ROI indicate the percentage of connections for this particular ROI (to every other functional parcellation ROI) showing significant connectivity based on *p*-value thresholding ($p<.05$) without the lowest AIC value across all four mixed-effect models.

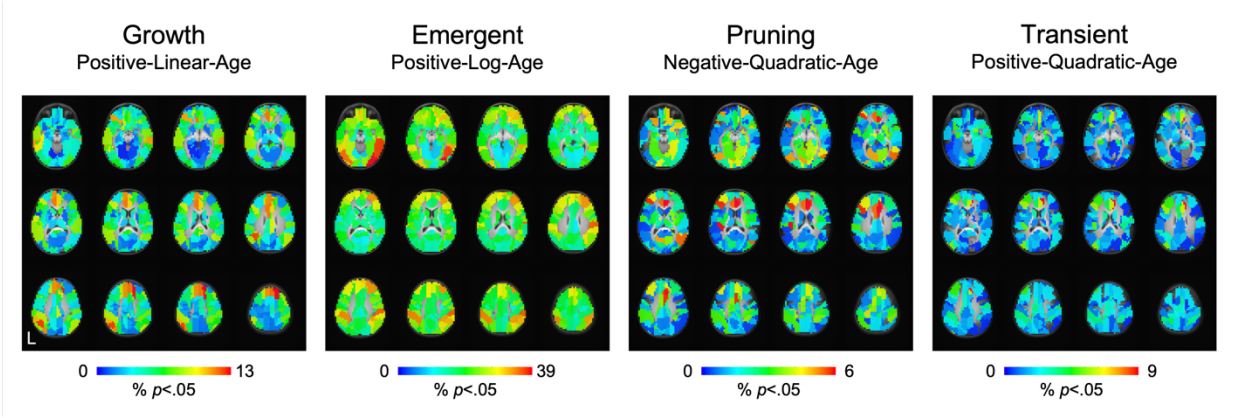

Figure S2. Heatmaps of age effects: Axial view. Qualitatively, heatmaps show unique patterns of age effects on brain connectivity across the first two years of life corresponding to growth (positive-linear-age), emergent (positive-log-age), pruning (negative-quadratic-age), and transient (positive-quadratic-age) effects. The color map and value of each ROI indicate the percentage of connections for this particular ROI (to every other functional parcellation ROI) showing significant connectivity based on *p*-value thresholding ($p<.05$) and the lowest AIC value across all four mixed-effect models.

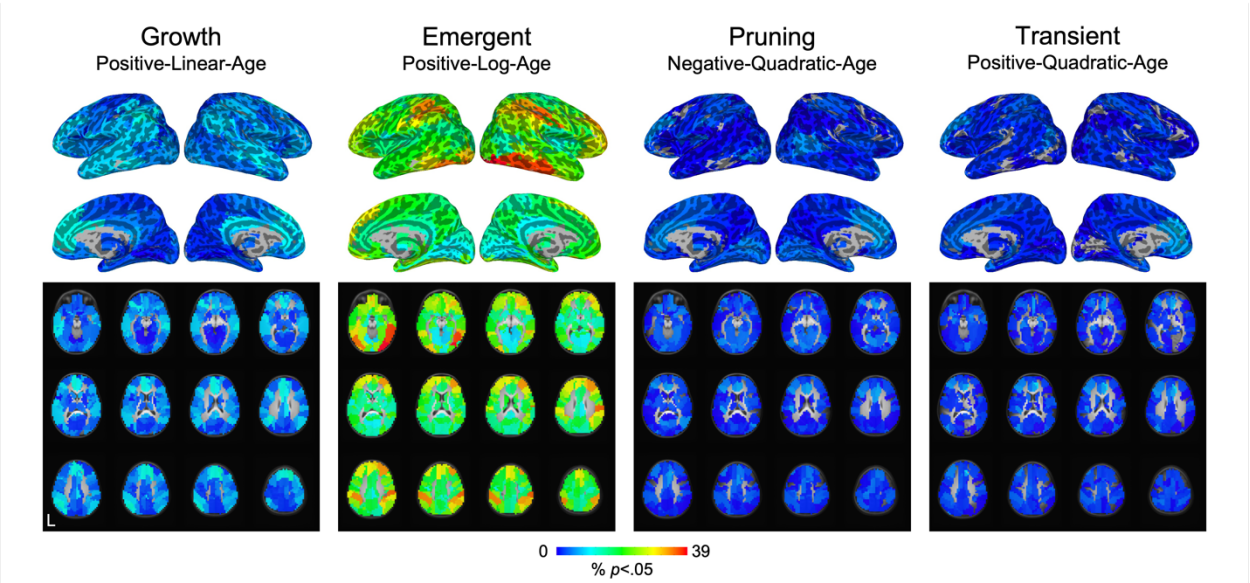

Figure S3. Heatmaps of age effects with consistent color range. Qualitatively, heatmaps show unique patterns of age effects on brain connectivity across the first two years of life corresponding to growth (positive-linear-age), emergent (positive-log-age), pruning (negative-quadratic-age), and transient (positive-quadratic-age) effects. The color map and value of each ROI indicate the percentage of connections for this particular ROI (to every other functional parcellation ROI) showing significant connectivity based on *p*-value thresholding ($p<.05$) and the lowest AIC value across all four mixed-effect models. The color range has been standardized across all four models to allow for quick comparison.

Whole Brain Heatmap Analysis with Full Length Data

Methods

We have previously demonstrated that three minutes of rsfMRI data (i.e., 90 volumes in our dataset) reliably yields underlying functional connectivity patterns (Salzwedel et al., 2019; Chen et al., 2021b, 2021a; Liu et al., 2021). However, to ensure that truncation did not influence the results, a supplemental whole brain heatmap analysis was conducted. Participant characteristics are reproduced from the main text with the additional inclusion of full rsfMRI scan length distribution for each time point (Table S1). Using the same methods as described in the main text, we characterized developmental trajectories in functional connectivity in the entire cohort with truncated data (i.e., main results) and full length data. Briefly, mixed-effect models included random intercept and slope terms with the effect estimate associated with age, log(age), positive quadratic age, or negative quadratic age being the principal variable of interest in each of the four mixed-effect models, respectively. Other participant characteristics were included as covariates of no interest, including full scan length, scanner, sex, mean residual framewise displacement (rFD), gestational age at birth, birthweight, twin status (i.e., whether or not the participant was part of a twin birth), atypical development (e.g., Chiari malformation, later diagnosis with neurodevelopmental disorders such as autism spectrum disorder [ASD] or attention-deficit/hyperactivity disorder [ADHD]), premature birth (defined as <37 weeks at birth), NICU stay (>24 hours), and maternal psychiatric diagnosis (e.g., with schizophrenia, bipolar disorder, major depressive disorder, or other psychosis). Significance was defined as $p<.05$ and the Akaike information criterion (AIC) was used to determine which mixed-effect model was the best fit for the data. A summary measure defined as the percentage of significant connections (at $p<.05$) with the lowest AIC value normalized by the total number of possible connections (i.e., 277) was calculated and assigned to the seed ROI. This process was repeated for all ROIs to generate a heatmap such that the resulting heatmaps for each developmental model indicated the spatial distribution of age effects on functional connectivity.

A summary measure defined as the percentage of significant connections at $p<.05$ with the lowest AIC value normalized by the total number of possible connections [i.e., 277] was calculated and assigned to the seed ROI. For each mixed-effect model, we examined the correlation between heatmaps with truncated data and full length data to assess consistency of results.

Results

Heatmaps illustrating different age effects in the entire cohort with truncated data (i.e., findings from main text reproduced here; Figures S4A and S5A) and full length data (Figures S4B and S5B) revealed highly similar patterns. Indeed, we observed high correlations between heatmaps with truncated data and heatmaps with full length data for all four mixed-effect models (growth: $r=.832$, $p<.001$; emergent: $r=.944$, $p<.001$; pruning: $r=.833$, $p<.001$; transient: $r=.829$, $p<.001$; Figure S6), indicating that results were highly consistent with and without truncation. Furthermore, the main pattern whereby the emergent model best captured growth in connectivity over the first two years was also replicated using the full length data (Figure S7). Taken together, these results demonstrate that growth trajectory patterns are robust and minimally impacted by rsfMRI data truncation.

Table S1. Participant Characteristics Including Full Length rsfMRI Scan.

	n=90
Sex (F/M)	47/43
Race (White/non-White)	56/34
Gestational Number (Singleton/Twin)	40/50
Atypical Development[a]	11
Mother Psychiatric Diagnosis	11
Mild Ventriculomegaly	2
Premature Birth (<37 weeks)	38
NICU Stay > 24 hours	26
Gestational Age at Birth (Weeks)	36.37 (2.86)
Birthweight (Grams)	2665.56 (630.66)
Mother's Age at Birth (Years)	29.96 (5.47)
Father's Age at Birth (Years)	33.13 (7.00)[b]
Maternal Education (Years)[c]	14.97 (3.66)
Neonate Scan	
Gestational Age at Scan (Days)	293.51 (16.02)
Scanner (Allegra/Trio)	82/8
Mean rFD (mm)	0.09 (0.02)
Full Scan Length (Volumes)	135.54 (14.35)
Full Scan Length (Minutes)	4.52 (0.48)
One-year Scan	
Gestational Age at Scan (Days)	654.06 (18.52)
Scanner (Allegra/Trio)	78/12
Mean rFD (mm)	0.09 (0.03)
Full Scan Length (Volumes)	143.60 (12.33)
Full Scan Length (Minutes)	4.79 (0.41)
Two-year Scan	
Gestational Age at Scan (Days)	1020.63 (20.80)
Scanner (Allegra/Trio)	64/26
Mean rFD (mm)	0.10 (0.03)
Full Scan Length (Volumes)	144.51 (10.09)
Full Scan Length (Minutes)	4.82 (0.34)

[a]Chiari malformation, later diagnosis with neurodevelopmental disorders such as autism spectrum disorder (ASD) or attention-deficit/hyperactivity disorder (ADHD); [b]N=85; [c]At enrollment; NICU: neonatal intensive care unit; rFD: residual framewise displacement.

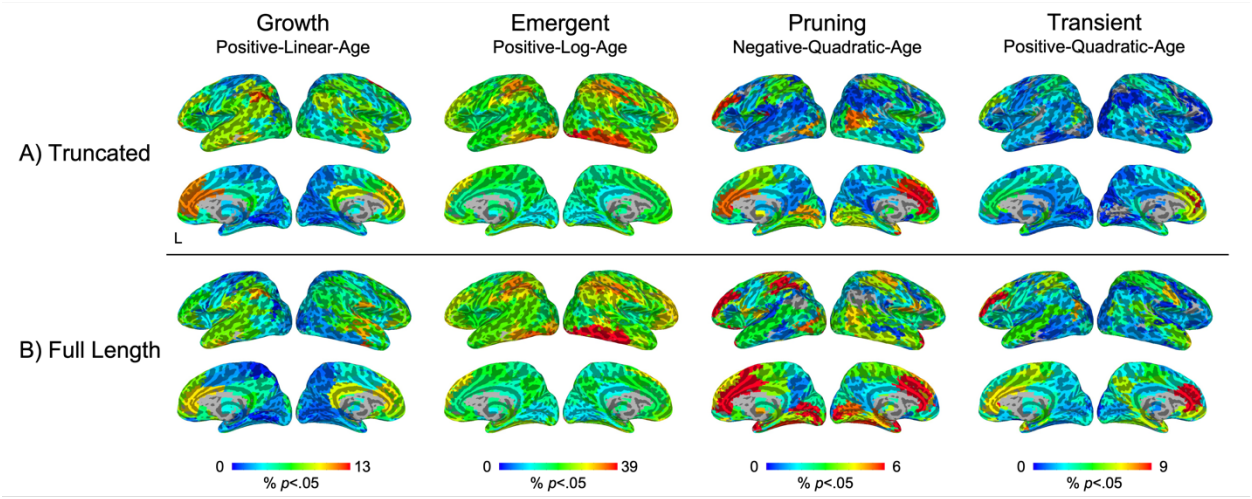

Figure S4. Heatmaps of age effects using truncated and full length data across the entire cohort. Heatmaps showing patterns of age effects on brain connectivity across the first year of life across the entire cohort using truncated data (A; reproduced from main text) and full length data (B). Similar patterns are observed for all four mixed-effect models, indicating that truncation minimally impacts growth trajectory patterns. The color map and value of each ROI indicate the percentage of connections for this particular ROI (to every other functional parcellation ROI) showing significant connectivity based on *p*-value thresholding ($p<.05$) and the lowest AIC value across all four mixed-effect modes.

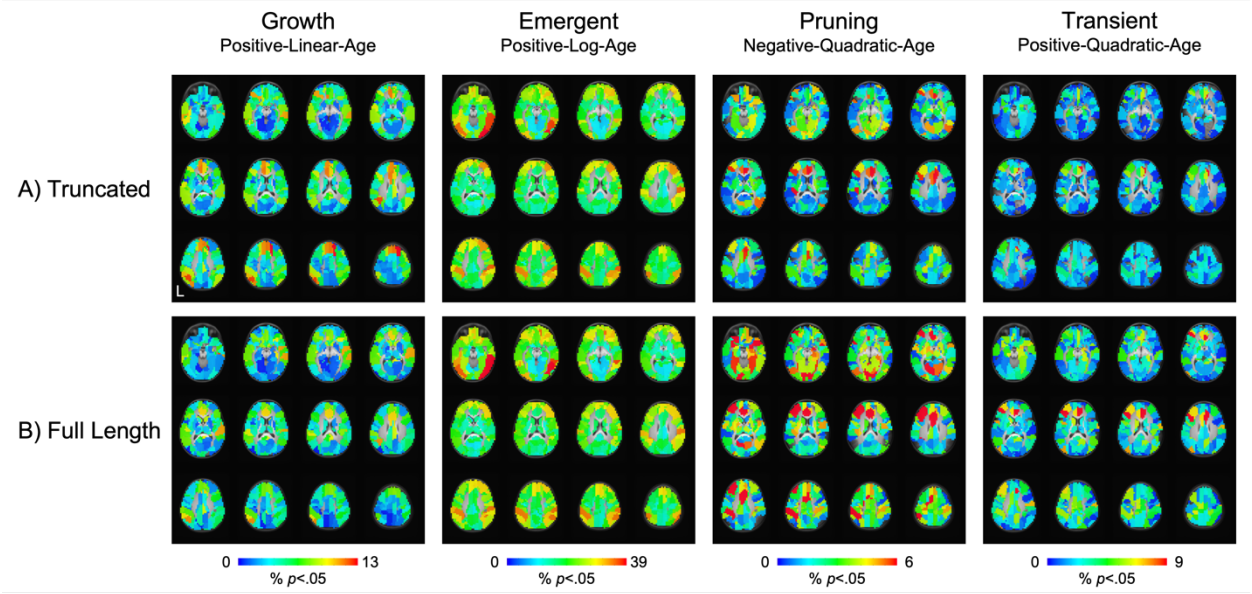

Figure S5. Heatmaps of age effects using truncated and full length data across the entire cohort: Axial view. Heatmaps showing patterns of age effects on brain connectivity across the first year of life across the entire cohort using truncated data (A; reproduced from main text) and full length data (B). Similar patterns are observed for all four mixed-effect models, indicating that truncation minimally impacts growth trajectory patterns. The color map and value of each ROI indicate the percentage of connections for this particular ROI (to every other functional parcellation ROI) showing significant connectivity based on *p*-value thresholding ($p<.05$) and the lowest AIC value across all four mixed-effect modes.

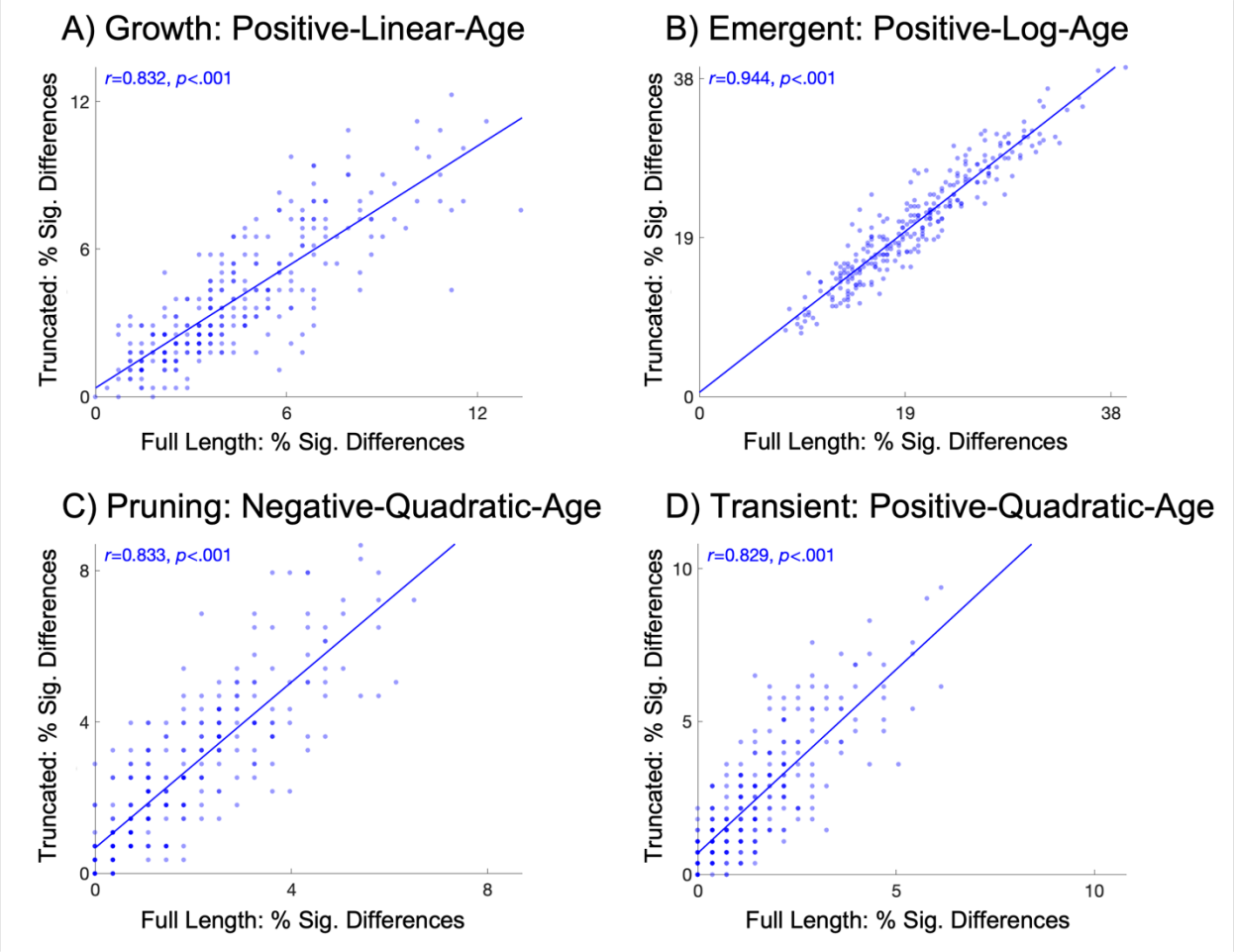

Figure S6. Correlations between heatmaps using truncated data and heatmaps using full length data for each age model. Strong correlations (i.e., high similarity) are observed for all four models including growth (A), emergent (B), pruning (C), and transient (D) models. This indicates that data truncation has minimal impact on the distribution of functional connectivity growth trajectories.

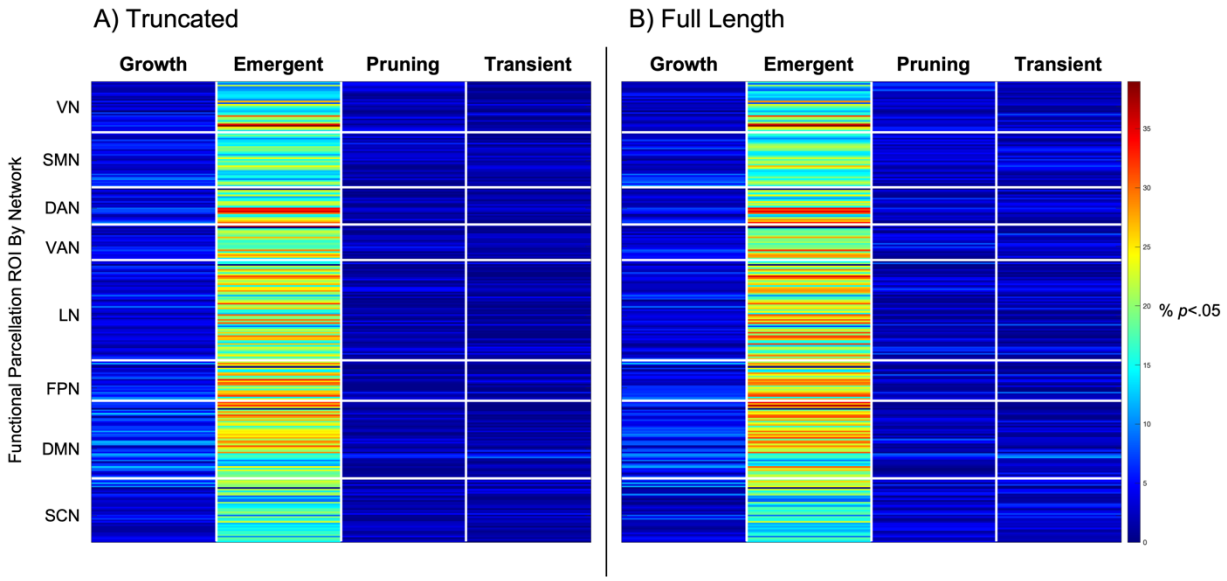

Figure S7. Emergent age effects consistently dominate with and without truncation. Across the four mixed-effect age models, the emergent model dominates growth trajectories in functional connectivity over the first two years of life in the entire cohort using truncated data (A; reproduced from main text) and full length data (B). Along the y-axis, each row corresponds to one ROI (out of a total of 278 ROIs in the 2-year functional parcellation atlas), organized by resting state network membership. The color map and value of each cell indicates the percentage of connections for this particular ROI (to every other functional parcellation ROI) showing significant connectivity based on *p*-value thresholding ($p<.05$) and the lowest AIC value across all four mixed-effect models. [VN: visual network; SMN: sensorimotor network; DAN: dorsal attention network; VAN: ventral attention network; LN: limbic network; FPN: frontoparietal network; DMN: default mode network; SCN: subcortical network]

Whole Brain Heatmap Analysis Stratified by Term Status

Methods

Given that preterm birth significantly impacts neurodevelopmental trajectories (Smyser et al., 2010; Pollatou et al., 2022), a supplemental whole brain heatmap analysis was conducted to assess whether term status influenced the results. Infants from the entire cohort were stratified based on term status (n=38 preterm defined as gestational age at birth <37 weeks, n=52 full term; Table S2). The whole brain heatmap analysis methods as described in the main text were implemented to characterize developmental trajectories in functional connectivity within these two subgroups. Briefly, mixed-effect models included random intercept and slope terms with the effect estimate associated with age, log(age), positive quadratic age, or negative quadratic age being the principal variable of interest in each of the four mixed-effect models, respectively. Other participant characteristics were included as covariates of no interest, including scanner, sex, mean residual framewise displacement (rFD), gestational age at birth, birthweight, twin status (i.e., whether or not the participant was part of a twin birth), atypical development (e.g., Chiari malformation, later diagnosis with neurodevelopmental disorders such as autism spectrum disorder [ASD] or attention-deficit/hyperactivity disorder [ADHD]), NICU stay (>24 hours), and maternal psychiatric diagnosis (e.g., with schizophrenia, bipolar disorder, major depressive disorder, or other psychosis). Significance was defined as $p<.05$ and the Akaike information criterion (AIC) was used to determine which mixed-effect model was the best fit for the data. A summary measure defined as the percentage of significant connections (at $p<.05$) with the lowest AIC value normalized by the total number of possible connections (i.e., 277) was calculated and assigned to the seed ROI. This process was repeated for all ROIs to generate a heatmap such that the resulting heatmaps for each developmental model indicated the spatial distribution of age effects on functional connectivity. For each mixed-effect model, we examined the correlation between heatmaps for full term and preterm subgroups to assess consistency of results within each subgroup.

In addition to using a *p*-value thresholding approach, an effect size thresholding approach was also implemented to avoid sample size biases among the subgroups analyzed and to ensure that the findings were not driven by the uneven distribution of subjects across the subgroups. For this, a Cohen's *d* effect size was calculated and a medium effect size ($d \geq .5$) was used as a threshold (Reddan et al., 2017; i.e., connections showing a medium or large effect size were included). A summary measure defined as the percentage of connections showing at least a medium effect size ($d \geq .5$) with the lowest AIC value normalized by the total number of possible connections (i.e., 277) was calculated and assigned to the seed ROI. This process was repeated for all ROIs to generate a heatmap such that the resulting heatmaps for each developmental model indicated the spatial distribution of age effects on functional connectivity.

Results

Heatmaps illustrating different age effects with *p*-value thresholding stratified by subgroups are shown in Figures S8 and S9 with the findings in the entire cohort from the main text reproduced here for comparison (top row in Figures S8A and S9A). Overall, patterns were similar across all three groups (entire cohort, full term, preterm). At the uncorrected level, across all three groups, growth effects were consistently localized to higher-order frontal, parietal, and temporal regions, as well as anterior cingulate gyrus. These effects were least prevalent in visual and subcortical areas. Emergent effects were also consistent across all three groups; these effects were dominant in visual, temporal, parietal, and sensorimotor areas and least prevalent in temporal, subcortical, and mid-cingulate regions. As in the entire cohort, pruning effects for both full term and preterm infants were localized to frontal and temporal areas as well as anterior cingulate gyrus and least present in primary temporal regions. Interestingly, the preterm subgroup qualitatively showed stronger pruning and transient effects compared with the full term subgroup. Indeed, correlations between full term and preterm subgroup heatmaps reflect this. Whereas strong correlations were observed for both growth (r=0.368, p<.001; Figure S10A) and emergent

effects (r=0.754, p<.001; Figure S10B), indicating high similarity between full term and preterm patterns for these models, weak correlations were observed for pruning (r=0.050, p<.001; Figure S10C) and transient (r=0.237, p<.001; Figure S10D) effects. Taken together, this indicates that preterm infants may drive the pruning and transient effects observed in the entire cohort. Future work should be conducted in larger sample sizes to validate and extend these findings.

One of the key findings in the entire cohort was that the emergent (positive-log-age) model best captured growth in connectivity (i.e., largest percentage of effects) over the first two years of life across the four mixed-effect models (Figure S11A; reproduced from main text Figure 3). Consistent with this, emergent age effects dominated in both full term (Figure S11B) and preterm (Figure S11C) subgroups such that emergent effects seem to dominate developmental trajectories regardless of term status.

Despite the difference in sample size (52 full term, 38 preterm), a similar distribution of age effects was observed for each subgroup based on p-value thresholds; this indicates that the effects observed within the preterm subgroup are likely associated with larger effect sizes. Indeed, by directly thresholding based on Cohen's d effect size (Figures S12 and S13), age-related effects observed in the preterm subgroup qualitatively showed the largest effect sizes compared with the full term subgroup as well as the entire cohort. This suggests that preterm infants may drive the age-related effects observed in the entire cohort; future work should validate these findings in larger sample sizes. Consistent with p-value thresholding results, the emergent (positive-log-age) model best captured growth in connectivity over the first two years of life in the entire cohort (Figure S14A) as well as in full term (Figure S14B) and preterm (Figure S14C) subgroups.

Table S2. Participant Characteristics Stratified by Term Status.

	Full term n=52	Preterm[a] n=38	*P*-value
Sex (F/M)	34/18	13/25	0.003
Race (White/non-White)	29/23	27/11	0.14
Gestational Number (Singleton/Twin)	33/19	7/31	<.001
Atypical Development[b]	6	5	1.00
Mother Psychiatric Diagnosis	8	3	0.34
Mild Ventriculomegaly	2	0	1.00
NICU Stay > 24 hours	3	23	<.001
Gestational Age at Birth (Weeks)	38.38 (1.14)	33.61 (2.07)	<.001
Birthweight (Grams)	3010.08 (451.59)	2194.11 (529.65)	<.001
Mother's Age at Birth (Years)	29.48 (5.46)	30.61 (5.50)	0.34
Father's Age at Birth (Years)	32.06 (4.82)[c]	34.58 (9.06)[d]	0.10
Maternal Education (Years)[e]	14.85 (3.63)	15.13 (3.75)	0.72
Neonate Scan			
Gestational Age at Scan (Days)	298.60 (16.32)	286.55 (12.81)	<.001
Scanner (Allegra/Trio)	47/5	35/3	1.00
Mean rFD (mm)	0.09 (0.03)	0.09 (0.02)	0.68
One-year Scan			
Gestational Age at Scan (Days)	657.25 (18.94)	649.68 (17.22)	0.06
Scanner (Allegra/Trio)	45/7	33/5	1.00
Mean rFD (mm)	0.09 (0.03)	0.10 (0.03)	0.19
Two-year Scan			
Gestational Age at Scan (Days)	1022.98 (22.29)	1017.42 (18.36)	0.21
Scanner (Allegra/Trio)	38/14	26/12	0.63
Mean rFD (mm)	0.10 (0.03)	0.11 (0.03)	0.32

[a]Preterm birth defined as gestational age at birth <37 weeks; [b]Chiari malformation, later diagnosis with neurodevelopmental disorders such as autism spectrum disorder (ASD) or attention-deficit/hyperactivity disorder (ADHD); [c]n=49; [d]n=36; [e]At enrollment; NICU: neonatal intensive care unit; rFD: residual framewise displacement.

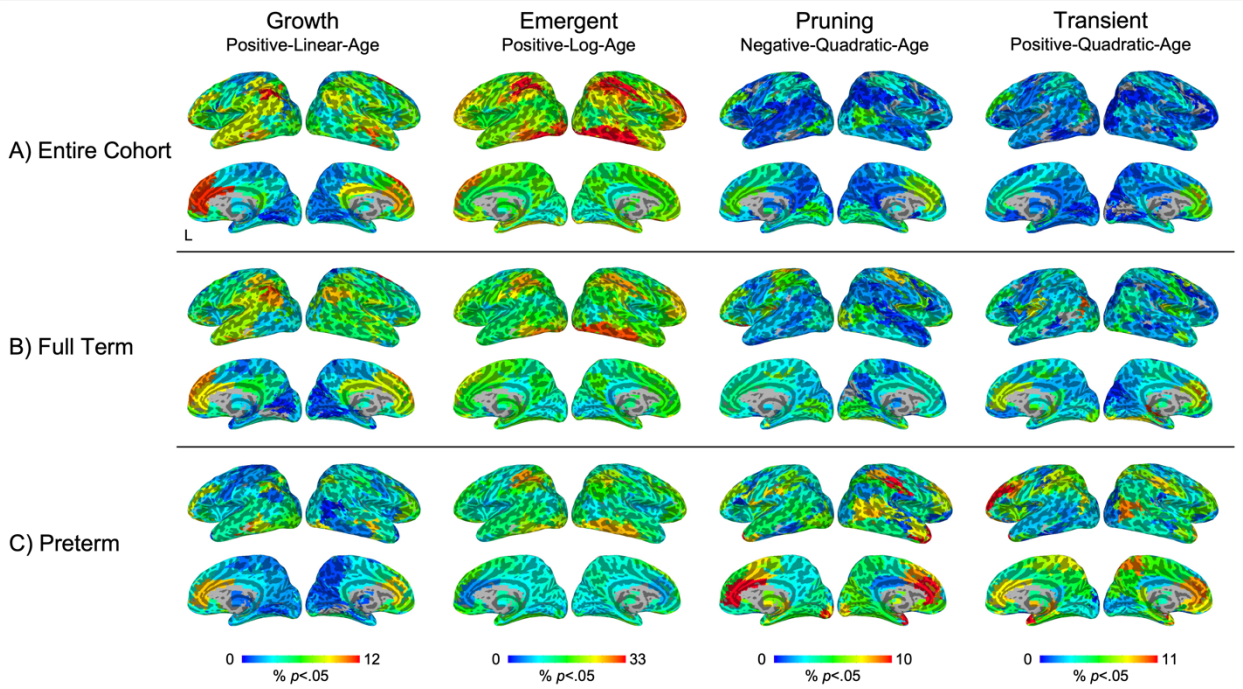

Figure S8. Heatmaps of age effects stratified by subgroup. Heatmaps showing patterns of age effects on brain connectivity across the first year of life across the entire cohort (n=90; A), full term subgroup (n=52; B), and preterm subgroup (n=38; C). Similar patterns are observed for growth (positive-linear-age) and emergent (positive-log-age) models across all three groups. Qualitatively, the preterm subgroup shows stronger pruning and transient effects compared with the full term subgroup, suggesting that preterm infants may drive the pruning and transient effects observed in the entire cohort. The color map and value of each ROI indicate the percentage of connections for this particular ROI (to every other functional parcellation ROI) showing significant connectivity based on *p*-value thresholding ($p<.05$) and the lowest AIC value across all four mixed-effect modes.

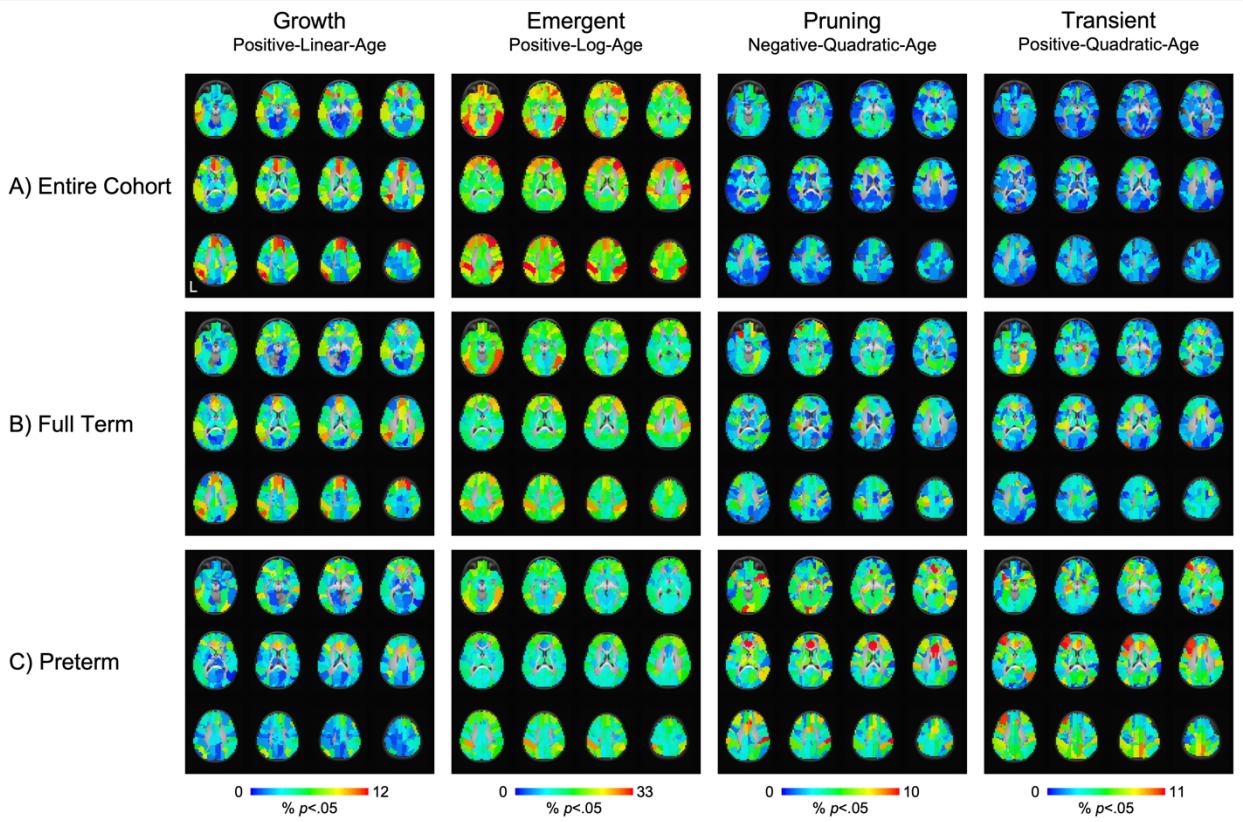

Figure S9. Heatmaps of age effects stratified by subgroup: Axial view. Heatmaps showing patterns of age effects on brain connectivity across the first year of life across the entire cohort (n=90; A), full term subgroup (n=52; B), and preterm subgroup (n=38; C). Similar patterns are observed for growth (positive-linear-age) and emergent (positive-log-age) models across all three groups. Qualitatively, the preterm subgroup shows stronger pruning and transient effects compared with the full term subgroup, suggesting that preterm infants may drive the pruning and transient effects observed in the entire cohort. The color map and value of each ROI indicate the percentage of connections for this particular ROI (to every other functional parcellation ROI) showing significant connectivity based on *p*-value thresholding ($p<.05$) and the lowest AIC value across all four mixed-effect modes.

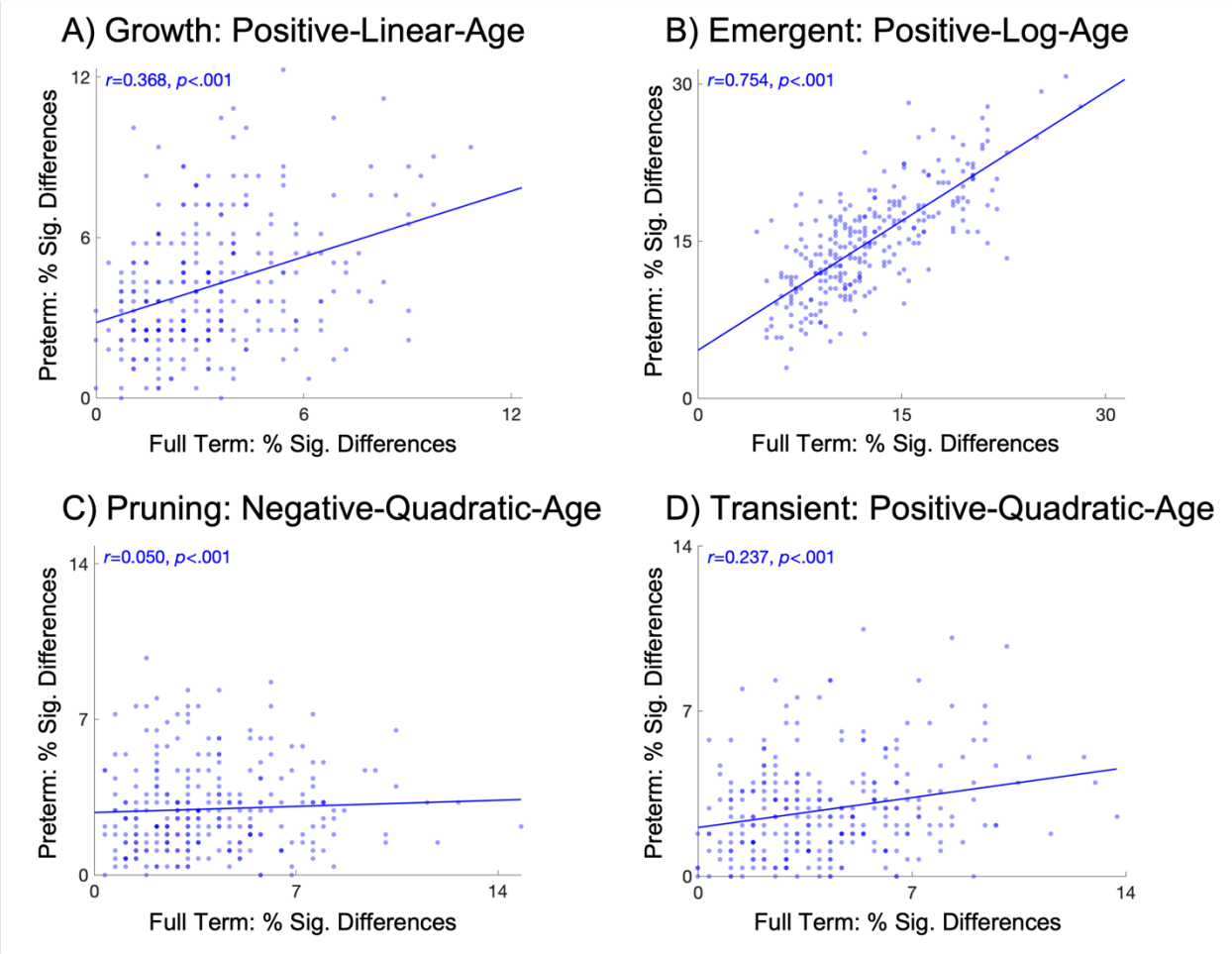

Figure S10. Correlations between full term and preterm heatmaps for each age model. Strong correlations (i.e., high similarity) are observed for growth (A) and emergent (B) models, but weak correlations (i.e., low similarity) are observed for pruning (C) and transient (D) models. This supports the notion that preterm infants may drive the pruning and transient effects observed in the entire cohort.

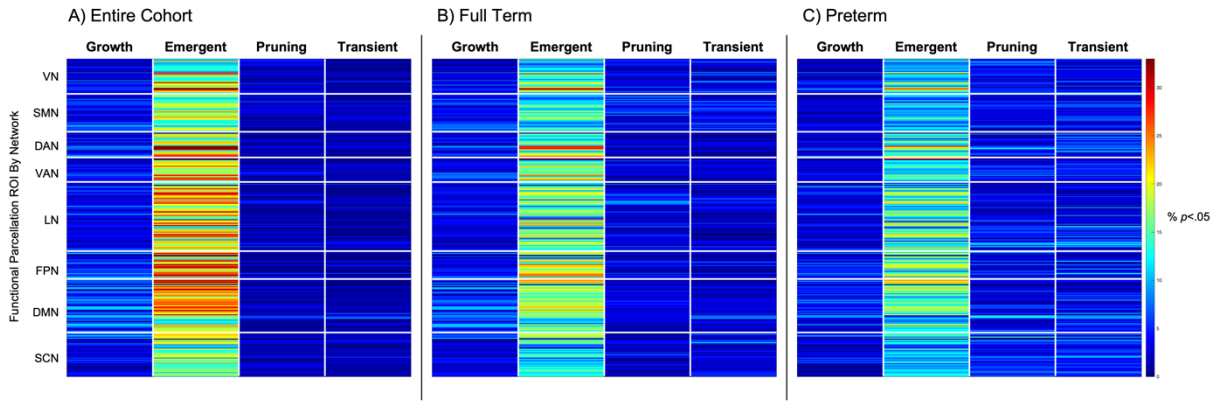

Figure S11. Emergent age effects consistently dominate regardless of term status. Across the four mixed-effect age models, the emergent model dominates growth trajectories in functional connectivity over the first two years of life in the entire cohort (n=90; A) as well as in the full term subgroup (n=52; B) and preterm subgroup (n=38; C). Along the y-axis, each row corresponds to one ROI (out of a total of 278 ROIs in the 2-year functional parcellation atlas), organized by resting state network membership. The color map and value of each cell indicates the percentage of connections for this particular ROI (to every other functional parcellation ROI) showing significant connectivity based on *p*-value thresholding ($p<.05$) and the lowest AIC value across all four mixed-effect models. [VN: visual network; SMN: sensorimotor network; DAN: dorsal attention network; VAN: ventral attention network; LN: limbic network; FPN: frontoparietal network; DMN: default mode network; SCN: subcortical network]

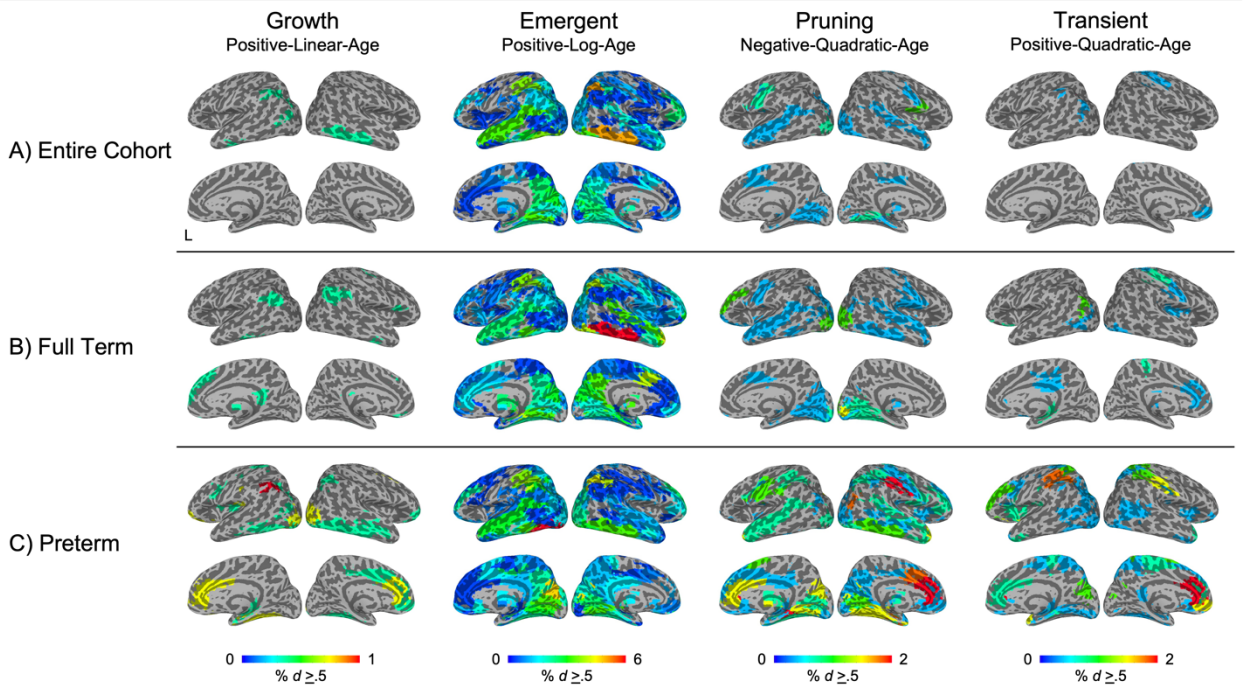

Figure S12. Heatmaps of age effects stratified by subgroup: Cohen's *d* thresholding. Heatmaps showing patterns of age effects on brain connectivity across the first year of life across the entire cohort (n=90; A), full term subgroup (n=52; B), and preterm subgroup (n=38; C). Qualitatively, the preterm subgroup shows the largest effect sizes compared with the full term subgroup as well as the entire cohort, suggesting that preterm infants may drive age-related effects observed in the entire cohort. The color map and value of each ROI indicate the percentage of connections for this particular ROI (to every other functional parcellation ROI) showing significant connectivity based on Cohen's *d* effect size thresholding ($d \geq .5$) and the lowest AIC value across all four mixed-effect modes.

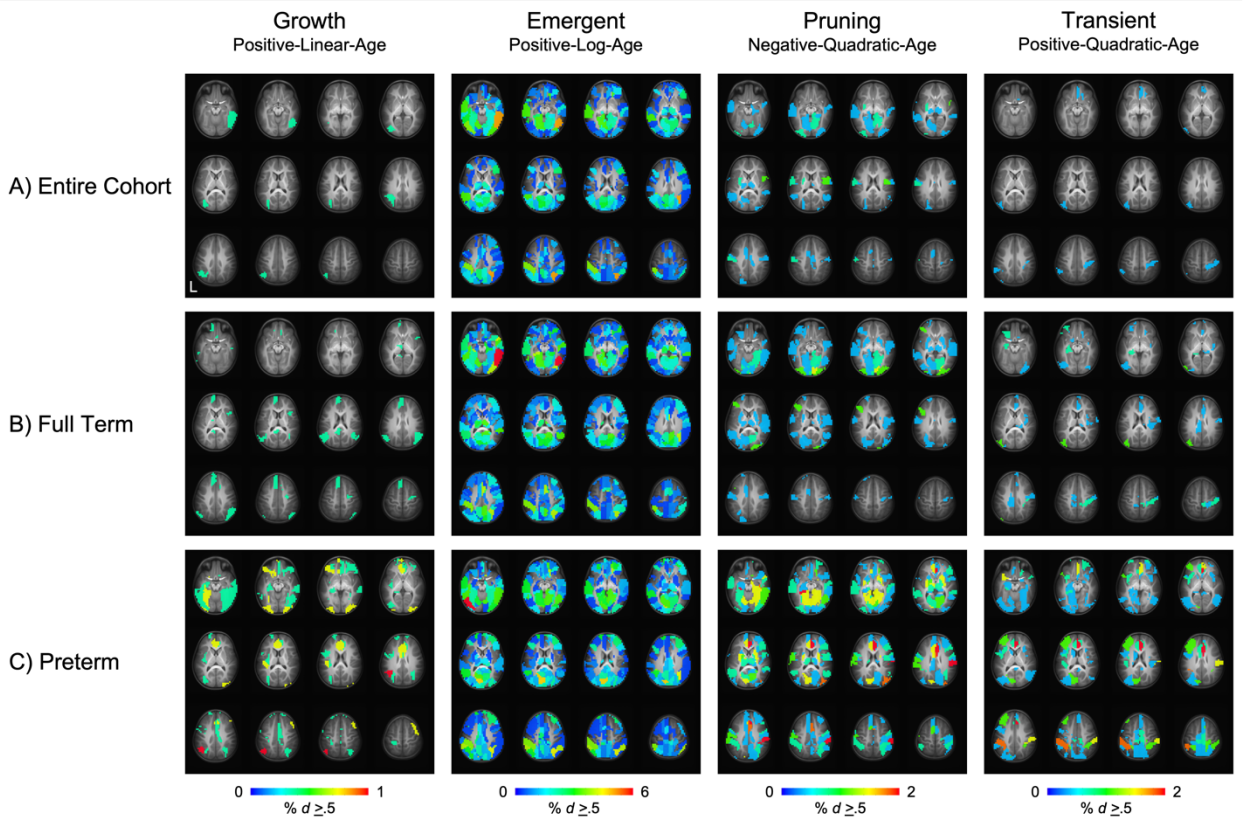

Figure S13. Heatmaps of age effects stratified by subgroup: Cohen's *d* thresholding, axial view. Heatmaps showing patterns of age effects on brain connectivity across the first year of life across the entire cohort (n=90; A), full term subgroup (n=52; B), and preterm subgroup (n=38; C). Qualitatively, the preterm subgroup shows the largest effect sizes compared with the full term subgroup as well as the entire cohort, suggesting that preterm infants may drive age-related effects observed in the entire cohort. The color map and value of each ROI indicate the percentage of connections for this particular ROI (to every other functional parcellation ROI) showing significant connectivity based on Cohen's *d* effect size thresholding ($d \geq .5$) and the lowest AIC value across all four mixed-effect modes.

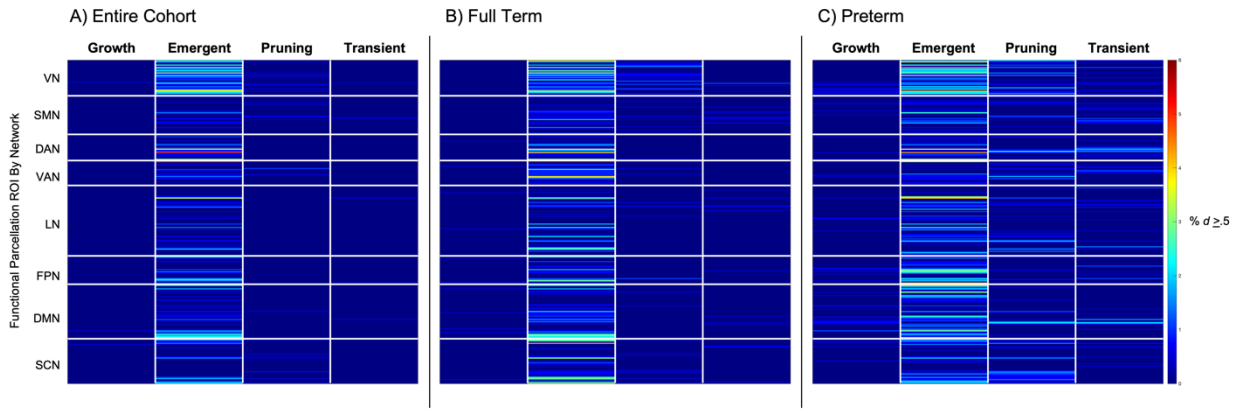

Figure S14. Emergent age effects consistently dominate with Cohen's *d* thresholding. Across the four mixed-effect age models, the emergent model dominates growth trajectories in functional connectivity over the first two years of life in the entire cohort (n=90; A) as well as in the full term subgroup (n=52; B) and preterm subgroup (n=38; C). Along the y-axis, each row corresponds to one ROI (out of a total of 278 ROIs in the 2-year functional parcellation atlas), organized by resting state network membership. The color map and value of each cell indicates the percentage of connections for this particular ROI (to every other functional parcellation ROI) showing significant connectivity based on Cohen's *d* effect size thresholding ($d \geq .5$) and the lowest AIC value across all four mixed-effect models. [VN: visual network; SMN: sensorimotor network; DAN: dorsal attention network; VAN: ventral attention network; LN: limbic network; FPN: frontoparietal network; DMN: default mode network; SCN: subcortical network]

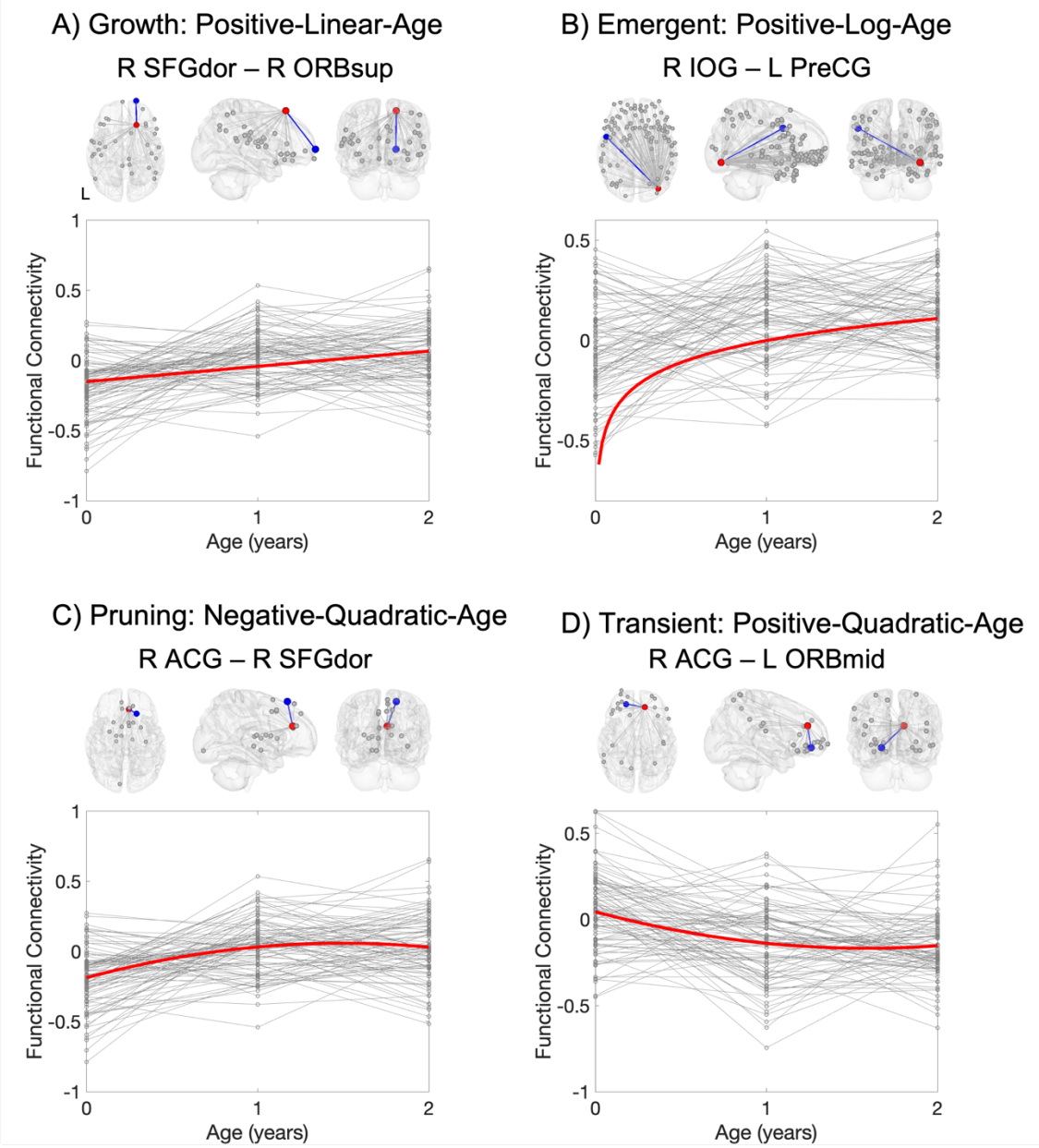

Figure S15. Representative connections for each mixed-effect model: Model fit curves. For better visualization, representative connections (in glass brain figure: representative connection denoted with blue line between red seed ROI to blue ROI) are plotted showing data from all subjects in gray with red model fit curve overlaid for the growth (A), emergent (B), pruning (C), and transient (D) models. [R SFGdor: right superior frontal gyrus, dorsal; R ORBsup: right orbitofrontal cortex, superior; R IOG: right inferior occipital gyrus; L PreCG: left precentral gyrus; R ACG: right anterior cingulate gyrus; L ORBmid: left orbitofrontal cortex, middle]

Table S3. ROI-Level Age Effects: Growth (Positive-Linear-Age)

Seed ROI	COG Coords			% Sig Connections	Connections (p_{FDR})
	x	y	z		
R SFGdor	26	36	29	12.27%	ANG-L (0.001), ANG-R (<0.001), HES-L (0.001), IFGoperc-R (<0.001), IFGtriang-L (0.035), INS-L (0.005), INS-R (<0.001), IPL-R (0.018), IPL-R (0.033), MCG-R (0.002), OLF-R (0.016), ORBinf-L (0.001), ORBinf-L (0.007), ORBinf-L (0.032), ORBinf-R (0.007), ORBinf-R (0.004), ORBinf-R (0.010), ORBmid-R (0.010), ORBsup-R (0.022), PAL-L (0.035), PCG-L (0.026), PCG-R (0.001), PCUN-R (0.007), REC-L (0.012), ROL-L (0.007), ROL-L (<0.001), ROL-L (<0.001), ROL-R (<0.001), STG-L (0.011), STG-L (0.003), STG-L (0.017), STG-R (0.050), STG-R (0.001), TPOsup-R (0.018)
L ANG	12	17	26	10.47%	FFG-L (0.031), FFG-L (0.048), FFG-R (0.007), IFGoperc-R (0.002), IOG-R (<0.001), ITG-L (0.017), ITG-L (<0.001), ITG-L (0.008), ITG-R (0.046), ITG-R (<0.001), ITG-R (0.047), MCG-R (0.048), MFG-L (<0.001), MFG-R (0.005), OLF (0.009), ORBinf-L (<0.001), ORBinf-L (0.003), ORBinf-R (<0.001), ORBmed-L (0.026), ORBmid-R (<0.001), ORBsup-R (0.002), ORBsup-R (0.017), ORBsup-R (<0.001), PoCG-R (<0.001), PreCG-L (0.002), PreCG-R (0.003), REC-L (0.003 REC-R (<0.001), SFGmed-L (0.014)
R SFGmed	23	38	28	9.03%	ANG-R (0.017), HES-L (<0.001), IFGoperc-L (0.002), IFGoperc-L (<0.001), IFGoperc-R (<0.001), IFGtriang-L (<0.001), IFGtriang-R (0.004), INS-L (<0.001), IPL-L (0.006), MCG-R (0.003), ORBinf-L (<0.001), ORBinf-L (0.048), ORBinf-R (<0.001), ORBinf-R (<0.001), ORBmid-R (0.030), ORBsup-L (0.001), ROL-L (0.048), ROL-R (<0.001), SMG-L (0.006), STG-L (<0.001), STG-L (<0.001), STG-L (<0.001), STG-L (<0.001), TPOsup-L (<0.001), TPOsup-R (<0.001)
L ACG	20	38	21	10.83%	HES-L (<0.001), HES-L (<0.001), HES-R (<0.001), INS-L (0.044), IPL-L (0.028), MCG-L (<0.001), MCG-R (0.015), PCG-L (0.017), PCG-R (0.035), PCL-L (<0.001), PCL-R (<0.001), PCUN-L (0.022), PHG-L (<0.001), PHG-R (<0.001), PoCG-L (<0.001), PoCG-R (<0.001), PreCG-L (<0.001), PreCG-R (<0.001), ROL-L (<0.001), ROL-L (0.003), SMG-L (0.012), SMG-L (0.029), SMG-R (0.012), SPG-L (0.017), SPG-R (0.008), STG-L (<0.001), STG-L (<0.001), STG-R (0.029), STG-R (<0.001), STG-R (<0.001)

COG Coords: Center of gravity coordinates. See Table S7 for list of automated-anatomical labeling (AAL) atlas region abbreviations.

Table S4. ROI-Level Age Effects: Emergent (Positive-Log-Age)

Seed ROI	COG Coords			% Sig Connections	Connections (p_{FDR})
	x	y	z		
R IOG	29	12	13	39.35%	AMYG-L (<0.001), AMYG-R (<0.001), ANG-R (<0.001), ANG-R (<0.001), CAU-L (<0.001), CAU-L (<0.001), CAU-R (<0.001), CAU-R (0.038), FFG-L (<0.001), FFG-L (0.005), FFG-R (<0.001), FFG-R (0.001), HIP-L (<0.001), HIP-L (0.025), HIP-R (0.006), IFGoperc-L (0.005), IFGoperc-L (0.028), IFGoperc-L (<0.001), IFGoperc-R (<0.001), IFGoperc-R (0.001), IFGoperc-R (<0.001), IFGoperc-R (<0.001), IFGtriang-L (<0.001), IFGtriang-L (<0.001), IFGtriang-L (<0.001), IFGtriang-R (<0.001), INS-R (0.007), IOG-L (<0.001), IPL-L (<0.001), IPL-L (<0.001), IPL-L (<0.001), IPL-R (<0.001), IPL-R (0.013), ITG-L (0.027), ITG-R (<0.001), MFG-R (0.030), MOG-L (<0.001), MOG-L (0.003), MOG-R (<0.001), MTG-L (0.007), MTG-L (0.023), MTG-R (0.025), MTG-R (0.002), MTG-R (0.048), MTG-R (0.038), MTG-R (<0.001), OLF-L (<0.001), OLF-R (<0.001), OLF-R (0.030), ORBinf-L (<0.001), ORBinf-L (<0.001), ORBinf-L (0.003), ORBinf-R (<0.001), ORBinf-R (<0.001), ORBinf-R (<0.001), ORBinf-R (<0.001), ORBinf-R (<0.001), ORBmed-L (<0.001), ORBmed-R (0.003), ORBmid-L (<0.001), ORBmid-L (0.017), ORBmid-L (<0.001), ORBmid-L (0.015), ORBmid-L (0.010), ORBmid-R (<0.001), ORBmid-R (0.007), ORBmid-R (0.001), ORBsup-L (<0.001), ORBsup-L (<0.001), ORBsup-L (0.005), ORBsup-R (<0.001), ORBsup-R (<0.001), ORBsup-R (<0.001), PAL-L (0.007), PAL-R (0.022), PHG-L (0.008), PHG-R (<0.001), PHG-R (<0.001), PHG-R (0.003), PoCG-L (0.021), PoCG-R (<0.001), PreCG-L (<0.001), PreCG-L (<0.001), PreCG-L (<0.001), PreCG-R (<0.001), PreCG-R (<0.001), REC-L (<0.001), REC-L (<0.001), REC-L (<0.001), REC-R (<0.001), REC-R (<0.001), REC-R (<0.001), REC-R (<0.001), ROL-R (0.012), SMG-R (<0.001), SOG-L (0.007), SPG-L (0.004), SPG-R (0.047), STG-L (<0.001), STG-R (0.002), TPOmid-L (0.003), TPOmid-L (<0.001), TPOmid-R (0.002), TPOsup-L (<0.001), TPOsup-L (<0.001), TPOsup-L (0.029), TPOsup-L (<0.001), TPOsup-R (<0.001), TPOsup-R (<0.001)
R ITG	33	20	13	36.46%	AMYG-L (0.002), AMYG-R (0.004), ANG-L (<0.001), ANG-R (<0.001), ANG-R (<0.001), CAU-L (<0.001), CAU-L (<0.001), CAU-R (<0.001), CAU-R (0.002), CAU-R (<0.001), FFG-L (0.002), FFG-L (<0.001), FFG-L (<0.001), FFG-L (0.002), FFG-L (<0.001), FFG-R (<0.001), FFG-R (<0.001), FFG-R (<0.001), FFG-R (<0.001), FFG-R (0.006), IFGoperc-R (0.018), IFGoperc-R (<0.001), IFGtriang-R (<0.001), INS-R (0.005), IOG-L (<0.001), IPL-L (<0.001), IPL-R (<0.001), ITG-L (<0.001), ITG-L (<0.001), ITG-L (<0.001), ITG-L (<0.001), ITG-L (<0.001), ITG-L (0.002), MFG-R (<0.001), MOG-L (<0.001), MOG-L (<0.001), MTG-L (0.003), MTG-L (<0.001), MTG-R (<0.001), OLF-R (<0.001), OLF-R (<0.001), ORBinf-L (<0.001), ORBinf-L (<0.001), ORBinf-R (<0.001), ORBinf-R (<0.001), ORBinf-R (<0.001), ORBinf-R (0.015), ORBinf-R (<0.001), ORBmid-L (<0.001), ORBmid-L (<0.001), ORBmid-L (<0.001), ORBmid-L (0.025), ORBmid-R (<0.001), ORBmid-R (0.002), ORBmid-R (<0.001), ORBsup-L (<0.001), ORBsup-L (<0.001), ORBsup-L (<0.001), ORBsup-L (0.031), ORBsup-R (<0.001), ORBsup-R (<0.001), ORBsup-R (<0.001), PHG-L (<0.001), PHG-L (<0.001), PHG-L (<0.001), PHG-L (0.002), PHG-L (0.005), PHG-R (<0.001), PHG-R (0.013), PHG-R (<0.001), PoCG-L (0.001), PoCG-R (<0.001), PreCG-L (<0.001), PreCG-R (0.046), PreCG-R (0.006), PreCG-R (<0.001), REC-L (<0.001), REC-L (0.010), REC-L (<0.001), REC-L (<0.001), REC-L (<0.001), REC-R (<0.001), REC-R (<0.001), REC-R (<0.001), REC-R (<0.001), REC-R (<0.001), REC-R (<0.001), ROL-L (<0.001), SMG-L (<0.001), SMG-L (0.009), SMG-R (<0.001), SOG-L (<0.001), SOG-L (<0.001), SPG-L (<0.001), SPG-R (<0.001), SPG-R (<0.001), TPOmid-L (<0.001), TPOmid-L (<0.001), TPOsup-L (0.020), TPOsup-L (<0.001), TPOsup-L (<0.001), TPOsup-R (<0.001)
R SMG	34	25	25	32.85%	ANG-L (<0.001), ANG-R (0.001), ANG-R (<0.001), CAU-L (<0.001), CAU-L (<0.001), CAU-R (<0.001), CAU-R (<0.001), CAU-R (0.007), FFG-R (0.017), FFG-R (0.003), FFG-R (0.041), IFGoperc-L (<0.001), IFGoperc-R (0.014), IFGoperc-R (0.023), IFGoperc-R (<0.001), IFGtriang-L (<0.001), IFGtriang-L (0.024), IFGtriang-R (<0.001), INS-L (0.014), INS-R (<0.001), IOG-R (<0.001), IPL-L (<0.001), IPL-L (<0.001), IPL-R (<0.001), IPL-R (<0.001), ITG-L (<0.001), ITG-L (<0.001), ITG-L (<0.001), ITG-L (0.003), ITG-L (0.001), ITG-R (0.014), MCG-L (0.005), MCG-R (<0.001), MCG-R (<0.001), MFG-L (<0.001), MFG-R (<0.001), MOG-L (0.014), MOG-L (<0.001), MOG-R (0.004), MOG-R (0.007), MTG-L (0.004), MTG-R (<0.001), MTG-R (0.044),

					MTG-R (<0.001), OLF-R (0.008), ORBinf-L (<0.001), ORBinf-L (<0.001), ORBinf-R (<0.001), ORBinf-R (<0.001), ORBinf-R (0.045), ORBinf-R (<0.001), ORBinf-R (0.004), ORBmid-L (0.016), ORBmid-L (<0.001), ORBmid-L (<0.001), ORBmid-L (<0.001), ORBmid-L (0.016), ORBmid-L (<0.001), ORBmid-R (<0.001), ORBmid-R (0.021), ORBmid-R (<0.001), ORBsup-L (<0.001), ORBsup-L (0.010), ORBsup-L (0.003), ORBsup-R (<0.001), ORBsup-R (0.013), PHG-L (<0.001), PreCG-L (<0.001), PreCG-L (<0.001), PreCG-L (0.012), PreCG-L (<0.001), PreCG-L (0.003), PreCG-R (0.026), PreCG-R (0.016), PreCG-R (0.036), PreCG-R (<0.001), REC-L (0.002), REC-R (<0.001), ROL-L (0.033), SFGdor-R (<0.001), SFGdor-R (<0.001), SFGdor-R (0.050), SFGmed-L (<0.001), SFGmed-R (<0.001), SMA-L (<0.001), SMA-R (<0.001), SMA-R (<0.001), SOG-L (0.002), SPG-L (<0.001), SPG-R (0.007), TPOsup-R (0.028)
L IOG	13	15	13	33.57%	AMYG-L (<0.001), AMYG-R (<0.001), ANG-R (0.001), ANG-R (<0.001), CAL-R (0.024), CAU-L (0.001), CAU-L (<0.001), CAU-R (<0.001), CAU-R (<0.001), FFG-L (<0.001), FFG-L (<0.001), FFG-L (<0.001), FFG-L (<0.001), FFG-L (<0.001), FFG-R (<0.001), FFG-R (<0.001), FFG-R (<0.001), FFG-R (0.004), IFGoperc-L (0.021), IFGoperc-L (0.024), IFGoperc-L (<0.001), IFGoperc-R (<0.001), IFGoperc-R (<0.001), IFGtriang-L (<0.001), IFGtriang-L (0.002), IFGtriang-L (<0.001), IFGtriang-R (<0.001), INS-L (0.002), INS-R (0.005), IOG-R (<0.001), IPL-L (<0.001), IPL-L (<0.001), IPL-L (<0.001), IPL-R (<0.001), IPL-R (<0.001), ITG-L (0.002), ITG-R (<0.001), LING-R (<0.001), MFG-R (0.013), MOG-L (<0.001), MOG-R (<0.001), MOG-R (<0.001), MTG-R (<0.001), ORBinf-L (<0.001), ORBinf-L (<0.001), ORBinf-L (<0.001), ORBinf-R (<0.001), ORBinf-R (<0.001), ORBinf-R (<0.001), ORBinf-R (0.002), ORBinf-R (0.021), ORBmid-L (<0.001), ORBmid-L (<0.001), ORBmid-L (<0.001), ORBmid-L (<0.001), ORBmid-L (0.028), ORBmid-R (<0.001), ORBmid-R (0.007), ORBmid-R (<0.001), ORBsup-L (0.005), ORBsup-L (<0.001), ORBsup-L (0.001), ORBsup-R (<0.001), ORBsup-R (<0.001), ORBsup-R (<0.001), PHG-L (<0.001), PHG-L (0.002), PHG-R (<0.001), PHG-R (<0.001), PHG-R (<0.001), PreCG-L (<0.001), PreCG-L (<0.001), PreCG-L (<0.001), PreCG-R (0.001), PreCG-R (<0.001), REC-L (0.006), REC-L (<0.001), REC-L (<0.001), REC-R (<0.001), REC-R (0.024), REC-R (<0.001), ROL-L (<0.001), ROL-L (0.004), SMG-R (<0.001), SOG-R (0.001), SPG-L (<0.001), SPG-R (<0.001), STG-L (0.006), TPOmid-L (0.049), TPOsup-L (0.015), TPOsup-L (0.048), TPOsup-L (<0.001), TPOsup-R (<0.001)

COG Coords: Center of gravity coordinates. See Table S7 for list of automated-anatomical labeling (AAL) atlas region abbreviations.

Table S5. ROI-Level Age Effects: Pruning (Negative-Quadratic-Age)

Seed ROI	COG Coords			% Sig Connections	Connections (p_{FDR})
	x	y	z		
R ACG	23	38	21	6.50%	ACG-L (<0.001), ACG-R (<0.001), CAL-L (<0.001), HIP-L (<0.001), HIP-R (<0.001), MCG-L (<0.001), MCG-R (<0.001), MCG-R (<0.001), PUT-L (<0.001), PUT-L (<0.001), PUT-R (<0.001), SFGdor-R (<0.001), SFGmed-L (<0.001), SFGmed-R (<0.001), SMA-R (<0.001), THA-L (<0.001), THA-L (<0.001), THA-R (<0.001)
L ROL	12	25	21	6.14%	ANG-L (<0.001), IFGtriang-L (<0.001), IFGtriang-R (<0.001), IPL-L (<0.001), ITG-L (<0.001), ITG-L (<0.001), MFG-L (<0.001), ORBinf-R (<0.001), ORBmid-R (<0.001), ORBsup-R (<0.001), ORBsup-R (<0.001), PreCG-L (0.002), PreCG-L (<0.001), PreCG-R (<0.001), SFGdor-L (<0.001), SFGdor-R (<0.001), SPG-L (<0.001)
L IFGtriang	13	38	21	5.78%	INS-L (<0.001), IPL-L (<0.001), IPL-R (<0.001), ORBinf-L (<0.001), ORBinf-L (<0.001), ORBmid-L (<0.001), ORBmid-L (<0.001), ORBsup-L (<0.001), PCUN-L (<0.001), PoCG-L (<0.001), PreCG-L (<0.001), PreCG-L (<0.001), ROL-L (<0.001), ROL-L (<0.001), SMA-L (<0.001), SPG-L (<0.001)
R ACG	24	39	21	5.78%	ACG-L (<0.001), ACG-R (<0.001), HIP-L (<0.001), HIP-L (<0.001), HIP-R (<0.001), MCG-R (<0.001), MCG-R (<0.001), OLF-L (<0.001), OLF-R (<0.001), ORBmed-R (<0.001), SFGdor-R (<0.001), SFGmed-L (<0.001), SFGmed-R (<0.001), SMA-R (<0.001), THA-L (<0.001), THA-R (<0.001)

COG Coords: Center of gravity coordinates. See Table S7 for list of automated-anatomical labeling (AAL) atlas region abbreviations.

Table S6. ROI-Level Age Effects: Transient (Positive-Quadratic-Age)

Seed ROI	COG Coords			% Sig Connections	Connections (p_{FDR})
	x	y	z		
R ACG	24	39	21	9.03%	HES-R (<0.001), IFGtriang-L (<0.001), IFGtriang-L (<0.001), IPL-L (<0.001), MFG-L (<0.001), ORBinf-L (<0.001), ORBinf-L (<0.001), ORBinf-R (<0.001), ORBinf-R (<0.001), ORBinf-R (<0.001), ORBmid-L (<0.001), ORBmid-L (<0.001), ORBmid-L (<0.001), ORBmid-L (<0.001), ORBmid-R (<0.001), ORBmid-R (<0.001), ORBsup-L (<0.001), ORBsup-L (<0.001), PCUN-L (<0.001), ROL-L (<0.001), ROL-R (<0.001), SMG-L (<0.001), SPG-L (<0.001), SPG-R (<0.001), TPOsup-R (<0.001)
R ORBmed	23	41	16	6.14%	ANG-L (<0.001), IFGtriang-L (<0.001), IPL-L (<0.001), IPL-L (<0.001), ORBinf-L (<0.001), ORBinf-L (<0.001), ORBinf-R (<0.001), ORBmid-L (<0.001), ROL-L (<0.001), SMG-L (<0.001), SMG-L (<0.001), SPG-L (<0.001), SPG-L (<0.001), SPG-R (<0.001), STG-L (<0.001), TPOsup-L (<0.001), TPOsup-R (<0.001)
R ACG	23	38	21	6.14%	IPL-L (<0.001), MFG-R (<0.001), ORBinf-L (<0.001), ORBinf-L (<0.001), ORBinf-R (<0.001), ORBinf-R (<0.001), ORBinf-R (<0.001), ORBinf-R (<0.001), ORBmid-L (<0.001), ORBmid-L (<0.001), ORBmid-R (<0.001), ORBmid-R (<0.001), ORBsup-L (<0.001), PCUN-L (<0.001), PCUN-R (<0.001), SPG-R (<0.001), SPG-R (<0.001)
L IFGtriang	13	38	21	5.78%	ACG-R (<0.001), FFG-R (<0.001), FFG-R (<0.001), ITG-L (<0.001), ITG-R (<0.001), ITG-R (0.001), MTG-R (<0.001), MTG-R (<0.001), ORBmed-R (<0.001), PHG-R (<0.001), SFGdor-R (<0.001), SFGmed-R (<0.001), TPOmid-L (<0.001), TPOmid-R (<0.001), TPOsup-L (<0.001), TPOsup-R (<0.001)

COG Coords: Center of gravity coordinates. See Table S7 for list of automated-anatomical labeling (AAL) atlas region abbreviations.

Table S7. Automated-Anatomical Labeling (AAL) Atlas Regions

Region	L/R	Abbreviation
Anterior cingulate gyrus	left	ACG-L
Anterior cingulate gyrus	right	ACG-R
Amygdala	left	AMYG-L
Amygdala	right	AMYG-R
Angular gyrus	left	ANG-L
Angular gyrus	right	ANG-R
Calcarine	left	CAL-L
Calcarine	right	CAL-R
Caudate	left	CAU-L
Caudate	right	CAU-R
Cuneus	left	CUN-L
Cuneus	right	CUN-R
Fusiform gyrus	left	FFG-L
Fusiform gyrus	right	FFG-R
Heschl gyrus	left	HES-L
Heschl gyrus	right	HES-R
Hippocampus	left	HIP-L
Hippocampus	right	HIP-R
Inferior frontal gyrus (operculum)	left	IFGoperc-L
Inferior frontal gyrus (operculum)	right	IFGoperc-R
Inferior frontal gyrus (triangular)	left	IFGtriang-L
Inferior frontal gyrus (triangular)	right	IFGtriang-R
Insula	left	INS-L
Insula	right	INS-R
Inferior occipital gyrus	left	IOG-L
Inferior occipital gyrus	right	IOG-R
Inferior parietal lobule	left	IPL-L
Inferior parietal lobule	right	IPL-R
Inferior temporal gyrus	left	ITG-L
Inferior temporal gyrus	right	ITG-R
Lingual gyrus	left	LING-L
Lingual gyrus	right	LING-R
Middle cingulate gyrus	left	MCG-L
Middle cingulate gyrus	right	MCG-R
Middle frontal gyrus	left	MFG-L
Middle frontal gyrus	right	MFG-R
Middle occipital gyrus	left	MOG-L
Middle occipital gyrus	right	MOG-R
Middle temporal gyrus	left	MTG-L
Middle temporal gyrus	right	MTG-R
Olfactory	left	OLF-L
Olfactory	right	OLF-R
Orbitofrontal cortex (inferior)	left	ORBinf-L
Orbitofrontal cortex (inferior)	right	ORBinf-R
Orbitofrontal cortex	left	ORBmed-L
Orbitofrontal cortex	right	ORBmed-R
Orbitofrontal cortex (middle)	left	ORBmid-L
Orbitofrontal cortex (middle)	right	ORBmid-R
Orbitofrontal cortex (superior)	left	ORBsup-L
Orbitofrontal cortex (superior)	right	ORBsup-R
Pallidum	left	PAL-L
Pallidum	right	PAL-R
Posterior cingulate gyrus	left	PCG-L
Posterior cingulate gyrus	right	PCG-R
Paracentral lobule	left	PCL-L
Paracentral lobule	right	PCL-R
Precuneus	left	PCUN-L
Precuneus	right	PCUN-R
ParaHippocampus gyrus	left	PHG-L
ParaHippocampus gyrus	right	PHG-R
Postcentral gyrus	left	PoCG-L
Postcentral gyrus	right	PoCG-R
Precentral gyrus	left	PreCG-L
Precentral gyrus	right	PreCG-R
Putamen	left	PUT-L
Putamen	right	PUT-R

Table S7 (cont'd). Automated-Anatomical Labeling (AAL) Atlas Regions

Region	L/R	Abbreviation
Rectus gyrus	left	REC-L
Rectus gyrus	right	REC-R
Rolandic operculum	left	ROL-L
Rolandic operculum	right	ROL-R
Superior frontal gyrus (dorsal)	left	SFGdor-L
Superior frontal gyrus (dorsal)	right	SFGdor-R
Superior frontal gyrus (medial)	left	SFGmed-L
Superior frontal gyrus (medial)	right	SFGmed-R
Supplementary motor area	left	SMA-L
Supplementary motor area	right	SMA-R
Supramarginal gyrus	left	SMG-L
Supramarginal gyrus	right	SMG-R
Superior occipital gyrus	left	SOG-L
Superior occipital gyrus	right	SOG-R
Superior parietal gyrus	left	SPG-L
Superior parietal gyrus	right	SPG-R
Superior temporal gyrus	left	STG-L
Superior temporal gyrus	right	STG-R
Thalamus	left	THA-L
Thalamus	right	THA-R
Temporal pole (middle)	left	TPOmid-L
Temporal pole (middle)	right	TPOmid-R
Temporal pole (superior)	left	TPOsup-L
Temporal pole (superior)	right	TPOsup-R

References

Chen H, Liu J, Chen Y, Salzwedel A, Cornea E, Gilmore JH, Gao W (2021a) Developmental heatmaps of brain functional connectivity from newborns to 6-year-olds. Dev Cogn Neurosci 50:100976 Available at: https://doi.org/10.1016/j.dcn.2021.100976.

Chen Y, Liu S, Salzwedel A, Stephens R, Cornea E, Goldman BD, Gilmore JH, Gao W (2021b) The subgrouping structure of newborns with heterogeneous brain-behavior relationships. Cereb Cortex 31:301–311.

Liu J, Chen Y, Stephens R, Cornea E, Goldman B, Gilmore JH, Gao W (2021) Hippocampal functional connectivity development during the first two years indexes 4-year working memory performance. Cortex 138:165–177 Available at: https://doi.org/10.1016/j.cortex.2021.02.005.

Pollatou A, Filippi CA, Aydin E, Vaughn K, Thompson D, Korom M, Dufford AJ, Howell B, Zöllei L, Martino A Di, Graham A, Scheinost D, Spann MN (2022) An ode to fetal, infant, and toddler neuroimaging: Chronicling early clinical to research applications with MRI, and an introduction to an academic society connecting the field. Dev Cogn Neurosci 54.

Reddan MC, Lindquist MA, Wager TD (2017) Effect size estimation in neuroimaging. JAMA Psychiatry 74:207–208.

Salzwedel AP, Stephens RL, Goldman BD, Lin W, Gilmore JH, Gao W (2019) Development of Amygdala Functional Connectivity During Infancy and Its Relationship With 4-Year Behavioral Outcomes. Biol Psychiatry Cogn Neurosci Neuroimaging 4:62–71 Available at: https://doi.org/10.1016/j.bpsc.2018.08.010.

Smyser CD, Inder TE, Shimony JS, Hill JE, Degnan AJ, Snyder AZ, Neil JJ (2010) Longitudinal analysis of neural network development in preterm infants. Cereb Cortex 20:2852–2862.